Hindawi
Shock and Vibration
Volume 2020, Article ID 6635011, 17 pages
https://doi.org/10.1155/2020/6635011

Research Article

A Dynamic Motion Tracking Control Approach for a Quadrotor Aerial Mechanical System

Hugo Yañez-Badillo,[1] **Francisco Beltran-Carbajal**,[2] **Ruben Tapia-Olvera**,[3] **Antonio Valderrabano-Gonzalez**,[4] **Antonio Favela-Contreras**,[5] **and Julio C. Rosas-Caro**[4]

[1]*Tecnológico de Estudios Superiores de Tianguistenco, División de Mecatrónica, Tianguistenco C.P. 52650, Estado de México, Mexico City, Mexico*
[2]*Universidad Autónoma Metropolitana, Unidad Azcapotzalco, Departamento de Energía, Azcapotzalco C.P. 02200, Mexico City, Mexico*
[3]*Universidad Nacional Autónoma de México, Departamento de Energía Eléctrica, C.P. 04510, Mexico City, Mexico*
[4]*Universidad Panamericana, Facultad de Ingeniería, Álvaro del Portillo 49, Zapopan, Jalisco 45010, Mexico*
[5]*Tecnologico de Monterrey, Escuela de Ingenieria y Ciencias, Monterrey, Nuevo León, Mexico*

Correspondence should be addressed to Francisco Beltran-Carbajal; fbeltran@azc.uam.mx

Received 3 October 2020; Revised 20 November 2020; Accepted 27 November 2020; Published 30 December 2020

Academic Editor: Pierangelo Masarati

Copyright © 2020 Hugo Yañez-Badillo et al. This is an open access article distributed under the Creative Commons Attribution License, which permits unrestricted use, distribution, and reproduction in any medium, provided the original work is properly cited.

This paper deals with the reference trajectory tracking problem and simultaneous active disturbance suppression on a class of controlled aerial mechanical systems by processing measurable output signals. A novel dynamic control method for desired motion reference trajectory tracking for quadrotor helicopters is introduced. Measurements of position output signals for efficient and robust tracking of motion profiles specified for the unmanned aerial vehicle are only required. Thus, differentiation of signals and real-time estimation of disturbances affecting the multi-input multioutput, underactuated nonlinear dynamic system are unnecessary. The presented active control approach can be directly extended for a class of vibrating mechanical systems. Analytical, experimental, and numerical results are presented to prove the satisfactory performance of the proposed trajectory tracking control approach for considerably perturbed operating scenarios.

1. Introduction

Interest in the study of unmanned aerial vehicles (UAVs) has increased in the last years since these aerial machines are able to accomplish several sorts of tasks. Diverse configurations of these vehicles can be found in multiple applications such as surveillance, monitoring, inspection, mapping, and payload transportation, among others [1, 2]. Efficient control of a four-rotor helicopter, commonly named quadrotor, has been addressed in various technological and scientific research works [3]. This vehicle is an underactuated nonlinear dynamic system because it counts with six degrees of freedom and only four independent control inputs. In contrast with other UAVs, such as the fixed-wing type that need large and wide space extensions for take-off and landing, a quadrotor has the ability of vertical take-off and landing (VTOL) which allows its safe operation indoors [4].

During flights, as a consequence of variable wind speeds, fluctuations in the surrounding humidity, and air resistance, quadrotors are subjected to endogenous and exogenous uncertainties due to a highly changing medium. A complex nonlinear dynamic behaviour between relevant variables and uncertainty is observed. Therefore, in order to efficiently perform trajectory tracking, slow and fast motion, hovering, stable flight, and VTOL, robust motion control schemes should be designed.

Numerous linear and nonlinear controllers have been proposed in the literature for quadrotor helicopters. In [5], PID and LQ control strategies have been implemented for stabilization of a quadrotor in presence of small perturbations. PID

control algorithms have been also introduced in [6], where results show a good flight performance for trajectory tracking at slow velocity in controlled environments. To regulate the rotational dynamics of a quadrotor in [7], a backstepping-based PID nonlinear control has been introduced, where the tracking error integral is used to minimize the steady-state error. The work in [8] deals with the regulation of the quadrotor position by using a robust PID controller, while robust attitude control is achieved by means of integral backstepping and terminal sliding modes.

Indeed, synthesis of several high-efficiency nonlinear control schemes may require accurate mathematical models or have a complex structure, which complicate their implementation in realistic systems due to some variables and parameters are unavailable or hard to obtain [9]. Thus, the Active Disturbance Rejection Control (ADRC) methodology constitutes an excellent alternative to achieve robustness against a wide class of disturbances [10]. Effective online disturbance estimation represents a fundamental component in ADRC [11, 12]. In this regard, in [13], disturbances are estimated by a Linear Extended State Observer (LESO) and then compensated by a PD controller. Authors in [14] propose an active disturbance rejection sliding mode controller, compensating estimates of uncertainties and external disturbances. Meanwhile, authors in [15] put all the available process information as an input in the control scheme for improving the disturbance estimation. In [16], satisfactory results to stabilize a quadrotor are achieved with a modified nonlinear version of ADRC.

In this paper, a new robust motion tracking control approach for a multiinput multioutput, underactuated nonlinear four-rotor helicopter is introduced. In contrast with other recent contributions, in the present dynamic tracking control proposal, additional designs of asymptotic extended state observers for real-time estimation of both disturbances and unavailable states signals are unnecessary. External disturbances and model uncertainties are actively suppressed through polynomial signal compensators, injected directly by suitable action of constrained, and reduced dynamic control inputs. Dynamic compensators are exploited to add outstanding active disturbance suppression capabilities. Integral structural reconstruction of unavailable time derivatives in the proposed control scheme is properly extended as well [17]. Effectiveness of integral reconstruction of velocity signals on efficiently controlled nonlinear vibrating systems has been proved in [18, 19]. Robustness of integral error action on electric motor control has been discussed in [20, 21]. In the present study, important insights for extension of the dynamic tracking control approach for a class of mechanical systems are also provided.

The remainder of this paper is organized as follows. In Section 2, an experimental case study on central ideas of the reference trajectory tracking control approach is described. The MIMO underactuated nonlinear dynamic model of the aerial vehicle is presented in Section 3. Then, active disturbance suppression is addressed by means of the proposed robust motion tracking control scheme in Section 4. In Section 5, three case studies are presented to demonstrate the efficiency and robustness of the introduced dynamic control scheme in presence of considerable disturbances. Lastly, conclusions and future work are highlighted in Section 6.

2. An Output Feedback Dynamic Control Approach

To depict the basic ideas of the proposed dynamic tracking control approach, consider the n Degree-of-Freedom (DOF) mass-spring-damper mechanical system shown in Figure 1. Here, x_i, $i = 1, 2, \ldots, n$, stands for position of the mass m_i, $y = x_1$ represents the output variable to be controlled, and u is a single force control input. Mass, damping, and stiffness parameters associated with the i-th DOF are denoted by m_i, k_i, and c_i, respectively.

The mathematical model of this multi-degree-of-freedom vibrating mechanical system is described by

$$\mathbf{M}\ddot{\mathbf{x}} + \mathbf{C}\dot{\mathbf{x}} + \mathbf{K}\mathbf{x} = \mathbf{u}, \tag{1}$$

where $\mathbf{M}$, $\mathbf{C}$, and $\mathbf{K}$ are, respectively, the mass, damping, and stiffness matrices given by

$$\mathbf{M} = \begin{bmatrix} m_1 & 0 & 0 & \ldots & 0 & 0 \\ 0 & m_2 & 0 & \ldots & 0 & 0 \\ \vdots & & \ddots & & & \\ 0 & 0 & 0 & \ldots & m_{n-1} & 0 \\ 0 & 0 & 0 & \ldots & 0 & m_n \end{bmatrix},$$

$$\mathbf{C} = \begin{bmatrix} c_1 & 0 & 0 & \ldots & 0 & 0 \\ 0 & c_2 & 0 & \ldots & 0 & 0 \\ \vdots & & \ddots & & & \\ 0 & 0 & 0 & \ldots & c_{n-1} & 0 \\ 0 & 0 & 0 & \ldots & 0 & c_n \end{bmatrix},$$

$$\mathbf{K} = \begin{bmatrix} k_1 + k_2 & -k_2 & 0 & \ldots & 0 & 0 & 0 \\ -k_2 & k_2 + k_3 & -k_3 & \ldots & 0 & 0 & 0 \\ \vdots & & & & & & \\ 0 & 0 & 0 & \ldots & -k_{n-1} & k_{n-1} + k_n & -k_n \\ 0 & 0 & 0 & \ldots & 0 & -k_n & k_n + k_{n+1} \end{bmatrix}, \tag{2}$$

with position vector $\mathbf{x} = [x_1 x_2 \ldots x_n]^T$ and control force vector $\mathbf{u} = [u \ 0 \ \ldots \ 0]^T$. Notice that equation (1) has been widely employed to model diverse engineering systems such as dynamic vibration absorbers [22, 23] and flexible structures [24].

Then, from equation (1), the following feedforward and feedback controller for asymptotic tracking of the desired reference position trajectory $y^*(t)$ can be synthesized:

$$u = m_1 \left[\ddot{y}_1^* - \beta_1 \left(\dot{y} - \dot{y}^* \right) - \beta_0 \left(y - y^* \right) - \xi(t) \right], \tag{3}$$

where β_0 and β_1 are control gains and $\xi(t)$ is disturbance affecting the dynamics of the actively controlled output variable y. Notice that $\xi(t)$ includes disturbances due to unmodeled dynamics and, possibly, parametric uncertainty and resonant excitation forces. Nevertheless, the trajectory tracking controller (3) requires measurements of position, velocity, and information of disturbances $\xi(t)$. Thus, the Generalized Proportional-Integral (GPI) control approach is used for the synthesis of a robust output feedback control scheme. This control technique

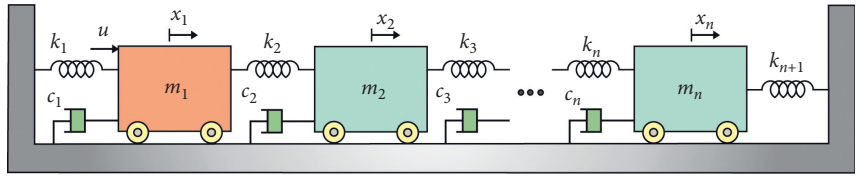

Figure 1: Schematic diagram of a n DOF flexible mechanical system.

is based on the integral reconstruction of the state variables through iterated integrations of the output and input variables [17]. Moreover, dynamic tracking error compensation is used to reject disturbances using only measurements of the output position variable y.

For control design purposes, it is assumed that the disturbance signal $\xi(t)$ can be approximated into a small window of time by the r-th order Taylor polynomial expansion, around a given time instant $t_0 > 0$,

$$\xi(t) \approx \sum_{i=0}^{r} p_i (t - t_0)^i, \tag{4}$$

where coefficients p_i are completely unknown. In addition, we have assumed that $\xi(t)$ is uniformly absolutely bounded, i.e.,

$$\|\xi\|_\infty = \sup_{t\in[0,\infty)} |\xi(t)| = \delta < \infty, \tag{5}$$

where δ is a possibly unknown positive constant.

Dynamics of the output position variable of the mechanical system is then described into an infinitesimal time window as

$$\ddot{y} = \frac{1}{m_1} u + \sum_{i=0}^{r} p_i (t - t_0)^i. \tag{6}$$

By integrating equation (6), one can obtain the following integral reconstructor for the velocity signal:

$$\hat{\dot{y}} = \frac{1}{m_1} \int_{t_0}^{t} u(\tau) \mathrm{d}\tau. \tag{7}$$

Note that initial conditions of the uncertain mechanical system and coefficients p_i were intentionally neglected in the integral reconstruction of the velocity signal. Thus, the structural estimate $\hat{\dot{y}}$ differs from the actual velocity signal by an algebraic polynomial up to $r+1$-th degree as follows:

$$\hat{\dot{y}} = \dot{y} + \sum_{i=0}^{r+1} \lambda_i (t - t_0)^i, \tag{8}$$

where constants λ_i depend on unknown initial conditions and coefficients of the disturbance model (4).

Then, a dynamic controller, using integral velocity reconstruction (7), for both active disturbance suppression and robust reference trajectory tracking is proposed as follows:

$$u = m_1 \left[\ddot{y}^* - \beta_{r+3} \left(\hat{\dot{y}} - \dot{y}^* \right) - \beta_{r+2} (y - y^*) - \chi_{r+1} \right], \tag{9}$$

with

$$\begin{aligned} \dot{\chi}_0 &= \beta_0 (y - y^*), \\ \dot{\chi}_1 &= \chi_0 + \beta_1 (y - y^*), \\ &\vdots \\ \dot{\chi}_r &= \chi_{r-1} + \beta_r (y - y^*), \\ \dot{\chi}_{r+1} &= \chi_r + \beta_{r+1} (y - y^*). \end{aligned} \tag{10}$$

Substitution of controller (9) into equation (6) leads to the closed-loop tracking error dynamics, $e = y - y^*$:

$$e^{(r+4)} + \sum_{k=0}^{r+3} \beta_k e^{(k)} = 0. \tag{11}$$

Hence, by selecting the design parameters β_k, the characteristic polynomial associated with the tracking error dynamics (11) is a Hurwitz polynomial results in a globally exponentially asymptotically stable equilibrium point. Therefore,

$$\lim_{t\longrightarrow\infty} e = 0 \Longrightarrow \lim_{t\longrightarrow\infty} y = y(t)^*. \tag{12}$$

2.1. Experimental Results. Analytical results were confirmed by real-time experiments performed on a three degree-of-freedom mass-spring-damper system characterized by the set of system parameters described in Table 1. The experimental setup used to test the proposed control approach is a rectilinear mechanical plant (Model 210a) provided by Educational Control Products. The design parameters for the output feedback tracking controller were selected to have the closed-loop characteristic polynomial:

$$P_c(s) = \left(s^2 + 2\zeta\omega_n s + \omega_n^2 \right)^4, \tag{13}$$

with $r = 4$, $\omega_n = 70$ rad/s, and $\zeta = 7$.

Figure 2 confirms the acceptable performance of the tracking control scheme. In this case study, the vibration test system was also perturbed by unmodeled dynamics associated with flexible beam structures connected to each mass, as shown in Figure 3. The satisfactory tracking of the reference position trajectory y^* is verified. This profile was planned to smoothly transfer the mass m_1 from the rest position to the equilibrium position of 0.01 m in a time interval of 3 s. Therefore, in Section 3, the proposed control approach is extended to the desired motion tracking problem on perturbed quadrotor helicopters.

3. Dynamic Model of a Quadrotor Helicopter

The quadrotor is a controlled aerial mechanical system with six degrees of freedom and only four control inputs. Moreover, its dynamic behaviour is governed by a set of strongly coupled

Table 1: Parameters of a 3 DOF mass-spring-damper system.

$m_1 = 2.82\,\text{kg}$	$c_1 = 3.64\,\text{Ns/m}$	$k_1 = 191.315\,\text{N/m}$
$m_2 = 2.59\,\text{kg}$	$c_2 = 1.75\,\text{Ns/m}$	$k_2 = 391.16\,\text{N/m}$
$m_3 = 2.59\,\text{kg}$	$c_3 = 1.75\,\text{Ns/m}$	$k_3 = 344.83\,\text{N/m}$

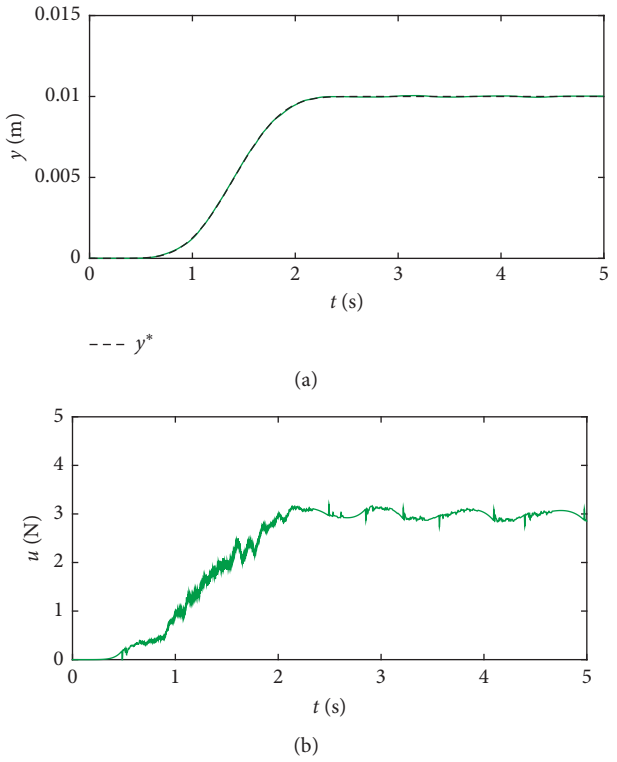

Figure 2: Experimental results for trajectory tracking planned for the controlled mass.

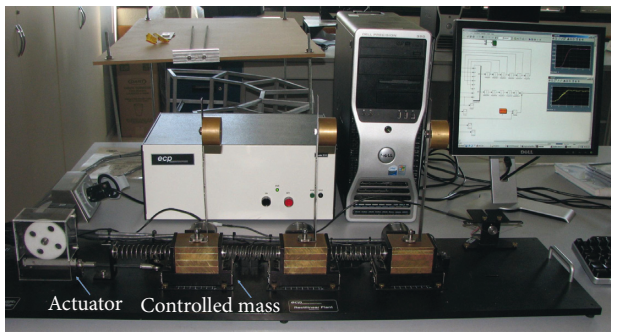

Figure 3: Configuration of the experimental setup used to test the performance of the proposed control approach.

nonlinear differential equations. A quadrotor is commonly designed to have a rigid body mechanical structure in order to obtain a simplified mathematical model, where two reference frames are used to describe its dynamic behaviour [3, 25]. The former, a global inertial coordinate system with X, Y, and Z axes, is attached to the Earth, and the second one with X', Y', and Z' axes fixed the quadrotor centre of mass as portrayed in Figure 4. Control force and torques, represented as u, τ_ψ, τ_θ, and τ_ϕ, are generated by four rotors located symmetrically in a suitably balanced mechanical structure. Thus, force and torque controllers should be synthesized to perform online and offline trajectory tracking for translation and rotation motion in the three-dimensional space.

Controlled system motion is achieved by increasing or decreasing properly the speed of each rotor. The pair of rotors 1 and 3 spin counterclockwise and the other in clockwise. Thus, pitching moment is produced by rotors 1 and 3, as shown in Figure 4(a). Similarly, rolling moment shown in Figure 4(b) is caused by the difference between forces produced by rotors 2 and 4. Yawing moment is originated when angular velocities of lateral rotors are modified, as displayed in Figure 4(c). On the contrary, the control force u, which allows lifting the quadrotor body, stands for the sum of all the vertical forces produced by each rotor.

Relation between produced forces by each rotor and control inputs is given by [3]

$$\begin{aligned} u &= \sum_{i=1}^{4} F_i, \\ \tau_\psi &= \sum_{i=1}^{4} \tau_{M_i}, \tau_\theta = (F_3 - F_1)l, \\ \tau_\phi &= (F_2 - F_4)l, \end{aligned} \tag{14}$$

where l is the distance from the motors to the centre of mass and τ_{M_i} stands for the torque induced by each electric motor M_i. F_i and τ_{M_i} are related to the geometry of the rotors blades by means of the coefficients of thrust and drag. Hence, motion in different directions on the plane can be attained by regulating angular velocities of rotors in order to change the magnitude of the forces F_i. Therefore, by suitably combining the rolling, pitching, and yawing moments, a quadrotor can track different reference trajectories.

The nonlinear dynamic model of the quadrotor is obtained by the Euler–Lagrange formalism [3, 25]. The vector of generalized coordinates is given by

$$q = [\, x \;\; y \;\; z \;\; \phi \;\; \theta \;\; \psi \,] \in \mathbb{R}^6, \tag{15}$$

where ϕ, θ, and ψ are the Euler angles describing the orientation of the system and x, y, and z are the position coordinates of the centre of mass measured with respect to the inertial reference frame. By considering the kinetic and potential energies, the Lagrangian is then given by

$$L = \frac{1}{2}\dot{\boldsymbol{\lambda}}\mathbf{M}\dot{\boldsymbol{\lambda}}^{\top} + \frac{1}{2}\dot{\boldsymbol{\eta}}^{\top}\mathfrak{J}\dot{\boldsymbol{\eta}} - \boldsymbol{\lambda}\mathbf{M}\mathbf{g}, \tag{16}$$

where $\mathbf{M}$ is the diagonal mass matrix, $\mathfrak{J}$ is the equivalent inertia tensor, $\mathbf{g} = [\, 0 \;\; 0 \;\; g \,]^{\top}$ is the gravity vector, g is the acceleration constant of gravity, $\lambda = [\, x \;\; y \;\; z \,]$ stands for the position vector, and $\eta = [\, \phi \;\; \theta \;\; \psi \,]$ is the orientation vector, both expressed in the global reference frame. The nonlinear translational dynamics of the quadrotor is given by

$$\begin{aligned} m\ddot{x} &= -u\sin\theta + \xi_x, \\ m\ddot{y} &= u\cos\theta\sin\phi + \xi_y, \\ m\ddot{z} &= u\cos\theta\cos\phi - mg + \xi_z, \end{aligned} \tag{17}$$

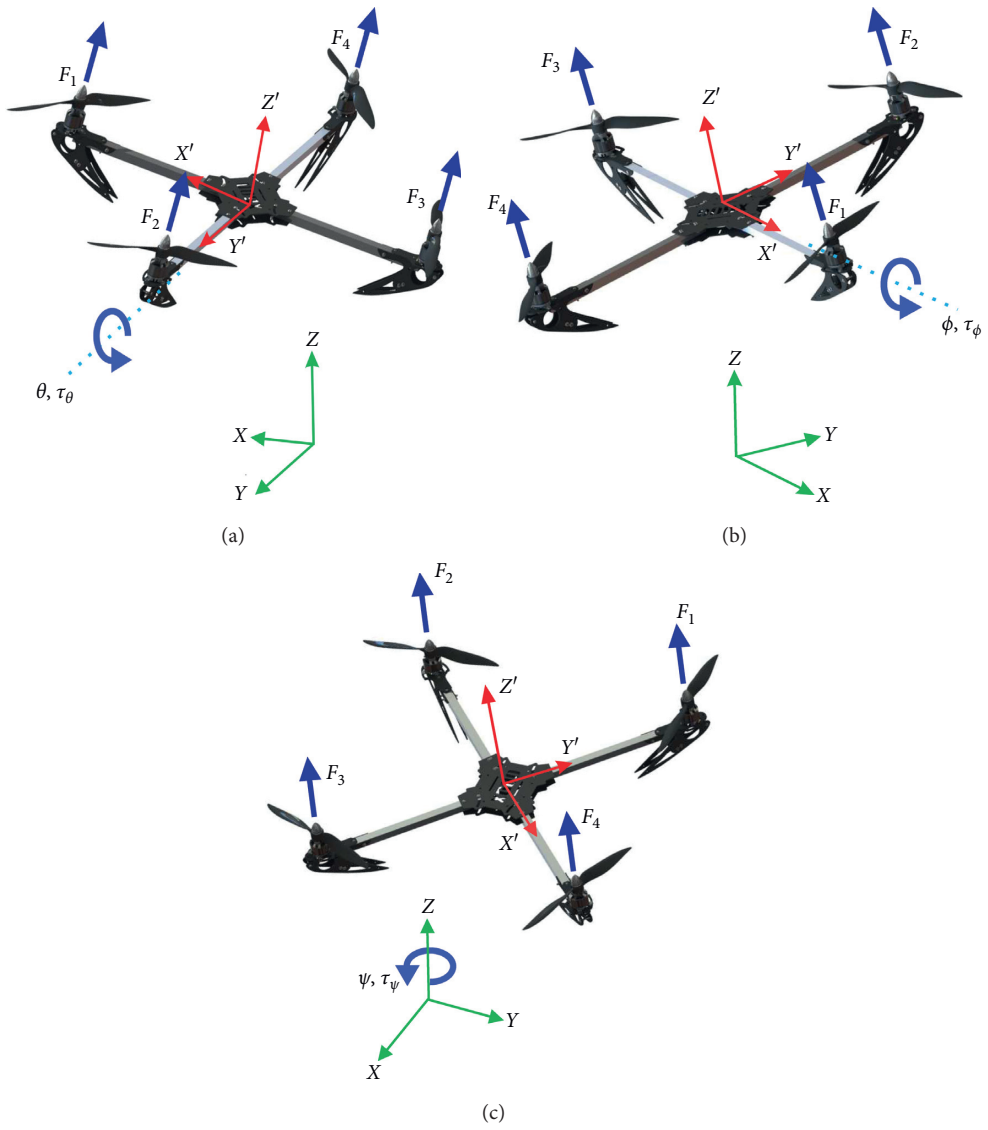

FIGURE 4: Motion in each direction of the space by the control inputs. (a) Pitching moment. (b) Rolling moment. (c) Yawing moment.

where ξ_x, ξ_y, and ξ_z denote unknown time-varying force disturbances affecting the operation of the aerial system. Simultaneously, rotational dynamics has numerous nonlinear couplings between system variables and parameters. Disturbed angular dynamics is described in a compact form as follows:

$$\mathfrak{J}\ddot{\boldsymbol{\eta}} = \boldsymbol{\tau}_{\boldsymbol{\eta}} - \mathbf{C}(\dot{\boldsymbol{\eta}}, t\eta\ )\dot{\boldsymbol{\eta}} + \boldsymbol{\xi}_{\boldsymbol{\eta}}, \tag{18}$$

where

$$\mathfrak{J} = \begin{bmatrix} -I_x s_\theta & 0 & I_x \\ (I_y - I_z)c_\theta c_\phi s_\phi & I_y c_\phi^2 + I_z s_\phi^2 & 0 \\ I_z c_\theta^2 c_\phi^2 + I_y c_\theta^2 s_\phi^2 + I_x s_\theta^2 & (I_y - I_z)c_\theta c_\phi s_\phi & -I_x s_\theta \end{bmatrix},$$
$$\mathbf{C}(\dot{\boldsymbol{\eta}}, \boldsymbol{\eta}) = \begin{bmatrix} c_{11} & c_{12} & c_{13} \\ c_{21} & c_{22} & c_{23} \\ c_{31} & c_{32} & c_{33} \end{bmatrix}, \tag{19}$$

with

$$
\begin{aligned}
c_{11} &= \left(I_z - I_y\right)\dot{\psi}s_\phi c_\phi c_\theta^2,\\
c_{12} &= -I_x\dot{\psi}c_\theta + I_y\left(\dot{\theta}s_\phi c_\phi + \dot{\psi}c_\theta s_\phi^2 - \dot{\psi}c_\theta c_\phi^2\right) - I_z\left(\dot{\psi}c_\theta s_\phi^2 - \dot{\psi}c_\theta c_\phi^2 + \dot{\theta}s_\phi c_\phi\right),\\
c_{13} &= 0,\\
c_{21} &= -I_x\dot{\psi}s_\theta c_\theta + I_y\dot{\psi}s_\theta c_\theta s_\phi^2 + I_z\dot{\psi}s_\theta c_\theta c_\phi^2,\\
c_{22} &= \left(I_z - I_y\right)\dot{\phi}s_\phi c_\phi,\\
c_{23} &= I_x\dot{\psi}c_\theta + I_y\left(-\dot{\theta}s_\phi c_\phi + \dot{\psi}c_\theta c_\phi^2 - \dot{\psi}c_\theta s_\phi^2\right) + I_z\left(\dot{\psi}c_\theta s_\phi^2 - \dot{\psi}c_\theta c_\phi^2 + \dot{\theta}s_\phi c_\phi\right),\\
c_{31} &= \dot{\theta}I_x s_\theta c_\theta + I_y\left(-\dot{\theta}s_\theta c_\theta s_\phi^2 + \dot{\phi}s_\phi c_\phi c_\theta^2\right) - I_z\left(\dot{\theta}s_\theta c_\theta c_\phi^2 + \dot{\phi}s_\phi c_\phi c_\theta^2\right),\\
c_{32} &= I_x\dot{\psi}s_\theta c_\theta - I_y\left(\dot{\theta}s_\theta s_\phi c_\phi + \dot{\phi}c_\theta s_\phi^2 - \dot{\phi}c_\theta c_\phi^2 + \dot{\psi}s_\theta c_\theta s_\phi^2\right) + I_z\left(\dot{\phi}c_\theta s_\phi^2 - \dot{\phi}c_\theta c_\phi^2 - \dot{\psi}s_\theta c_\theta c_\phi^2 + \dot{\theta}s_\theta s_\phi c_\phi\right),\\
c_{33} &= -I_x\dot{\theta}c_\theta + \left(I_y - I_z\right)\left(\dot{\psi}c_\theta^2 s_\phi c_\phi\right).
\end{aligned}
\tag{20}
$$

Here, for purposes of simplicity of the model representation, s_i and c_i stand for the sine and cosine functions for $i = \theta, \phi$. The control torque vector is denoted by $\tau_\eta = \begin{bmatrix}\tau_\phi & \tau_\theta & \tau_\psi\end{bmatrix}^\intercal$. Similarly, $\xi_\eta = \begin{bmatrix}\xi_\phi & \xi_\theta & \xi_\psi\end{bmatrix}^\intercal$ represents a torque disturbance vector due to wind corrupting the rotational dynamics. Parametric uncertainty and unmodeled dynamics could be also lumped in disturbances ξ_γ, for $\gamma = x, y, z, \phi, \theta, \psi$.

4. Robust Motion Tracking Control for Quadrotor Helicopters

ADRC focuses on the input and output evolution instead of the use of some detailed nonlinear mathematical model of the disturbed dynamic system [11, 12]. An extended state observer is designed to estimate disturbances. After, real-time estimated disturbances are included in the control syntheses to guarantee active disturbance rejection. In the present contribution, from a different control design perspective, disturbance observers and time derivatives of output signals are unnecessary. Time-varying disturbances are actively and directly suppressed by dynamic error compensation properly embedded into control signals.

The proposed main control scheme is schematically depicted in Figure 5. Two virtual controllers are synthesized for adjusting the nonactuated dynamics and ensure the efficient and robust tracking of position reference trajectories in X and Y directions. Meanwhile, fully actuated dynamics are regulated directly by suitable action of four robust controllers. The control scheme is based on tracking errors given by the difference between real measured variables and desired reference trajectories, with $\gamma = x, y, z, \phi, \theta, \psi$,

$$e_\gamma = \gamma - \gamma^*, \tag{21}$$

where the superscript * is used to denote reference trajectory for some system variable. Here, a virtual control block computes the reference trajectories θ^* and ϕ^*, according to the desired motion for X and Y directions as follows:

$$
\begin{aligned}
\theta^* &= \sin^{-1}\left(-\frac{1}{u}mv_x\right),\\
\phi^* &= \sin^{-1}\left(\frac{1}{u\cos\theta}mv_y\right).
\end{aligned}
\tag{22}
$$

For robust control design purposes, from equations (17) and (18), disturbed tracking error dynamics is simplified as

$$\ddot{e}_\gamma = v_\gamma + \xi_\gamma(t). \tag{23}$$

Similarly, $\xi_\gamma(t)$ are considered as bounded time-varying disturbance signals and locally approximated into a small interval of time by the r-th order Taylor polynomial expansions:

$$\xi_\gamma(t) \approx \sum_{i=0}^{r} p_{i,\gamma}\left(t - t_0\right)^i, \tag{24}$$

where coefficients $p_{i,\gamma}$ are assumed to be completely unknown.

From equation (23), integral reconstructors for velocity signals of tracking errors can be then computed by

$$\hat{\dot{e}}_\gamma = \int_{t_0}^{t} v_\gamma \mathrm{d}t. \tag{25}$$

The polynomial relationship between structural estimates $\hat{\dot{e}}_\gamma$ and actual velocity tracking error signals is given by

$$\hat{\dot{e}}_\gamma = \dot{e}_\gamma + \sum_{i=0}^{r+1} \lambda_{i,\gamma}\left(t - t_0\right)^i, \tag{26}$$

where parameters $\lambda_{i,\gamma}$ are also assumed to be unknown.

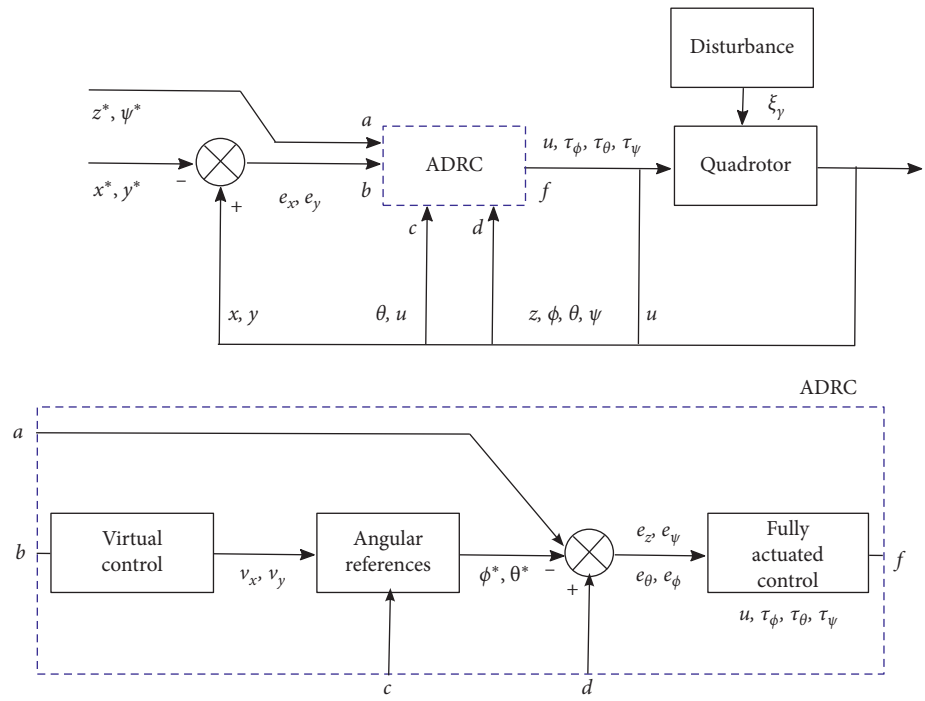

Figure 5: Main robust motion control scheme for a disturbed aerial quadrotor vehicle.

Auxiliary controllers for desired motion trajectory tracking tasks on the aerial vehicle are then proposed as

$$v_\gamma = -\beta_{r+3,\gamma}\hat{\tilde{e}}_\gamma - \beta_{r+2,\gamma}e_\gamma - \chi_{r+1,\gamma}, \tag{27}$$

with

$$\begin{aligned}
\dot{\chi}_{0,\gamma} &= \beta_{0,\gamma}e_\gamma,\\
\dot{\chi}_{1,\gamma} &= \chi_{0,\gamma} + \beta_{1,\gamma}e_\gamma,\\
&\vdots\\
\dot{\chi}_{r,\gamma} &= \chi_{r-1,\gamma} + \beta_{r,\gamma}e_\gamma,\\
\dot{\chi}_{r+1,\gamma} &= \chi_{r,\gamma} + \beta_{r+1,\gamma}e_\gamma.
\end{aligned} \tag{28}$$

Then, from equations (23) and (27), closed-loop tracking error dynamics is governed by

$$e_\gamma^{(r+4)} + \sum_{k=0}^{r+3}\beta_{k,\gamma}e_\gamma^{(k)} = 0. \tag{29}$$

Therefore, control gains $\beta_{k,\gamma}$ should be selected so that characteristic polynomials associated with the closed-loop error dynamics (29),

$$P_{\mathrm{CL},\gamma}(s) = s^{r+4} + \sum_{k=0}^{r+3}\beta_{k,\gamma}s^k, \tag{30}$$

are Hurwitz polynomials and faster than disturbance signals. In this way, reference trajectory tracking can be achieved:

$$\lim_{t\longrightarrow\infty} e_\gamma = 0 \Longrightarrow \lim_{t\longrightarrow\infty} \gamma = \gamma^*, \tag{31}$$

with $\gamma = x, y, z, \phi, \theta, \psi$.

Notice from (18) that

$$\ddot{\boldsymbol{\eta}} = \mathfrak{J}^{-1}\left[\boldsymbol{\tau}_{\boldsymbol{\eta}} - \mathbf{C}(\dot{\boldsymbol{\eta}}, \boldsymbol{\eta})\dot{\boldsymbol{\eta}}\right] + \mathfrak{J}^{-1}\boldsymbol{\xi}_{\boldsymbol{\eta}}. \tag{32}$$

The control torque vector can be then proposed as follows:

$$\boldsymbol{\tau}_{\boldsymbol{\eta}} = \mathfrak{J}\mathbf{v}_{\boldsymbol{\eta}} + \mathbf{C}(\dot{\boldsymbol{\eta}}, \boldsymbol{\eta})\dot{\boldsymbol{\eta}} + \mathfrak{J}\ddot{\boldsymbol{\eta}}^*, \tag{33}$$

with $\mathbf{v}_\eta = [v_\phi v_\theta v_\psi]^\intercal$. Thus, substitution of (33) into (18) yields

$$\begin{aligned}
\ddot{\boldsymbol{\eta}} &= \ddot{\boldsymbol{\eta}}^* + \mathbf{v}_{\boldsymbol{\eta}} + \mathfrak{J}^{-1}\boldsymbol{\xi}_{\boldsymbol{\eta}},\\
\ddot{\boldsymbol{e}}_{\boldsymbol{\eta}} &= \mathbf{v}_{\boldsymbol{\eta}} + \mathfrak{J}^{-1}\boldsymbol{\xi}_{\boldsymbol{\eta}},
\end{aligned} \tag{34}$$

and by expressing the angular acceleration disturbance vector as $\mathfrak{J}^{-1}\xi_{\boldsymbol{\eta}} = \mathbf{d}_{\boldsymbol{\eta}}$, it results

$$\ddot{\boldsymbol{e}}_{\boldsymbol{\eta}} = \mathbf{v}_{\boldsymbol{\eta}} + \mathbf{d}_{\boldsymbol{\eta}}, \tag{35}$$

which presents the structure in (23). Therefore, the control inputs for desired motion trajectory tracking and active disturbance suppression are proposed as

$$\begin{aligned}
u &= \frac{1}{\cos\phi\cos\theta}(mv_z + mg),\\
\tau_\phi &= k_\phi v_\phi,\\
\tau_\theta &= k_\theta v_\theta,\\
\tau_\psi &= k_\psi v_\psi,
\end{aligned} \tag{36}$$

with

$$k_\phi = I_x,$$
$$k_\theta = I_y \cos^2\phi + I_z \sin^2\phi, \quad (37)$$
$$k_\psi = I_z \cos^2\theta \cos^2\phi + I_y \cos^2\theta \sin^2\phi + I_x \sin^2\theta.$$

5. Case Studies on Dynamic Performance Assessment

In this section, numerical experiments to confirm the effectiveness of the proposed dynamic tracking control scheme are described. Experiments were implemented on a lightly damped quadrotor with parameters described in Table 2. Translational reference trajectories in meters are given by

$$x^*(t) = 2\sin\left(\frac{t}{2}\right)\cos\left(\frac{t}{4}\right),$$
$$y^*(t) = 2\sin\left(\frac{t}{2}\right)\sin\left(\frac{t}{4}\right), \quad (38)$$
$$z^*(t) = \frac{t}{4}.$$

Control design parameters were selected for matching closed-loop Hurwitz (stable) polynomials:

$$P_{\mathrm{CL},\gamma}(s) = \left(s^2 + 2\zeta_\gamma \omega_{n,\gamma} s + \omega_{n,\gamma}^2\right)^2 \left(s + p_{c,\gamma}\right), \quad (39)$$

Table 2: Parameters of the quadrotor system.

Parameter	Value	Units
m	1.016	kg
l	0.225	m
I_x	0.012450	kg·m^2
I_y	0.013303	Kg·m^2
I_z	0.024752	kg·m^2

with $\omega_{n,\gamma}$, ζ_γ, $p_{c,\gamma} > 0$ and $\gamma = x, y, z, \phi, \theta, \psi$. Controller adjustment parameters to perform a satisfactory robust tracking of planned trajectories were then selected as $\omega_{n,x} = \omega_{n,y} = 3$ rad/s, $\zeta_x = \zeta_y = 1$, and $p_{c,x} = p_{c,y} = 3$ rad/s; $\omega_{n,z} = 3$ rad/s, $\zeta_z = 2$, and $p_{c,z} = 2$ rad/s; $\omega_{n,\phi} = \omega_{n,\theta} = 10$ rad/s, $\zeta_\phi = \zeta_\theta = 3$, and $p_{c,\theta} = 10$ rad/s; and $\omega_{n,\psi} = 10$ rad/s, $\zeta_\psi = 1$, and $p_{c,\psi} = 10$ rad/s. Additionally, for purposes of robustness assessment, control input gains were selected as $k_\phi = I_x$, $k_\theta = I_y$, and $k_\psi = I_z$.

During simulation experiments, the quadrotor was exposed to follow planned trajectories in presence of completely unknown considerable external disturbances. For purposes of control robustness assessment, the wind disturbance models affecting the aerial vehicle dynamics described in [8, 26] were selected. Interested readers in more details about these disturbance models applied on controlled aerial vehicles can refer to the contributions [8, 26] and references therein. Three case studies for robustness and effectiveness assessment were thus developed.

In the first case study, the quadrotor is exposed to disturbances induced by wind gusts, similar as authors in [8]. Here, the effects of wind gusts on the quadrotor translational accelerations are considered:

$$f_{d_i}(t) = \begin{cases} 0, & 0 \le t \le 15, \\ 0.8\sin\left[\dfrac{\pi(t-30)}{31}\right] + 0.4\sin\left[\dfrac{\pi(t-30)}{7}\right] & \\ & 15 < t \le 45, \\ +0.08\sin\left[\dfrac{\pi(t-30)}{2}\right] + 0.056\sin\left[\dfrac{\pi(t-30)}{11}\right], & \\ 0, & 45 < t \le 65, \\ 0.8\sin\left[\dfrac{\pi(t-30)}{31}\right] + 0.4\sin\left[\dfrac{\pi(t-30)}{7}\right] & \\ & 65 < t \le 85, \\ +0.08\sin\left[\dfrac{\pi(t-30)}{2}\right] + 0.056\sin\left[\dfrac{\pi(t-30)}{11}\right], & \\ 0, & t > 85. \end{cases} \quad (40)$$

Therefore, the external disturbance forces introduced in (17) are defined such that

$$\xi_i = m f_{d_i}(t), \quad (41)$$

for $i = x, y, z$. Meantime, disturbance torques in (18) are the following:

$$\boldsymbol{\xi}_{\boldsymbol{\eta}} = \mathfrak{T}\left[\sin(t) + 0.2\sin(100\pi t)\right]. \tag{42}$$

On the contrary, in the second study, the quadrotor is subjected to the effects of crosswind disturbances. The crosswind representation is similar to that in [26], where authors introduce a wind speed model which directly perturbs the helicopter translational motion, and is given by

$$\begin{aligned} \xi_x &= -w_1 \sin\theta, \\ \xi_y &= w_1 \cos\theta \sin\phi, \\ \xi_z &= w_1 \cos\theta \cos\phi, \end{aligned} \tag{43}$$

where w_1 is the representation of the wind disturbance. Here, induced normal forces for each rotor are included. Additionally, the forces are related with the wind speed model as $w_1 = V_w(t)$, and $V_w(t) = V_{wg}(t) + V_{wt}(t)$, with

$$V_{wg}(t) = \begin{cases} 0, & t < T_{sg}, \\ A_g - A_g \cos\left(2\pi \dfrac{t - T_{sg}}{T_{eg} - T_{sg}}\right), & T_{sg} \le t \le T_{eg}, \\ 0, & T_{eg} < t, \end{cases} \tag{44}$$

where $V_w(t)$ is the wind speed expression composed by a gust component V_{wg} and a turbulence term V_{wt}, A_g is the amplitude of the wind gust, T_{sg} is its starting time, and T_{eg} is its stopping time. In this paper, values for $A_g = 1$ m/s, $T_{sg} = 30$ s, and $T_{eg} = 65$ s are adopted. Also, for representing the turbulence component V_{wt}, a band-limited white noise has been implemented. Enforced crosswind affecting rotational displacements is given by $\xi_\eta = [\, w_2 \;\; w_3 \;\; w_4 \,]^\intercal$, with $w_2 = 0.75 w_1$, $w_3 = 0.25 w_1$, and $w_4 = 0.15 w_1$ (cf. [26]).

In Figure 6, the above main disturbance features are depicted. Notice the differences in the representation for each case.

Exhaustive numerical experiments were performed for both case studies. Figure 7 depicts the vertical trajectory tracking in presence of wind gust and crosswinds, respectively. An adequate position tracking is achieved due to the robustness of the proposed controllers for facing unknown external disturbances. Also, it is appreciated that there is only a slight deviation in the tracking of the planned trajectories represented by discontinuous lines.

Notice from Figure 8 the proper tracking of the planned reference trajectories for X and Y directions, as a consequence of a suitable tuning of the virtual controllers. Moreover, as confirmed in Figure 9, the planned X-Y path is followed adequately by the quadrotor even in presence of the disturbances. Additionally, due to the features of the controller design, the error dynamic presents an asymptotically stable behaviour.

The path reference and the path following in X-Y-Z directions are portrayed in Figures 10(a) and 10(b), respectively. For purposes of simplicity in the representation, the results are presented only for case 1. Nevertheless, the proposed control scheme allows to achieve satisfactory results in both cases studies even though disturbances present diverse behaviour, crosswind, and wind gust, respectively.

Figures 11 and 12 show the control inputs responses calculated online to regulate efficiently the quadrotor flight according to planned trajectories and paths, as well as to reject uncertain variable disturbances in spite of not having information about their dynamic behaviour. Additionally, the proposed control scheme allows ensuring a proper tracking even though the information about the derivatives of the interest variables is not available.

Notice that actuators are not saturated by the computed control inputs, since these are acceptably small and smooth, which could represent considerable energy savings during the execution of flight tasks as well. Disturbance effects are also observed in each designed control input signal.

Figure 13 shows the time histories of the quadrotor pitch and roll tracking. The references θ^* and ϕ^* were computed online accordingly to equation (22) in order to regulate the displacements in X and Y directions adequately. In both cases the tracking of the computed references is achieved due to the robust structure of the proposed control scheme, where the virtual control stage depends on the regulation and tracking of this variables for ensuring the planned path following.

Lastly, the desired yaw angle reference ψ^* is given as follows:

$$\psi^* = \begin{cases} \psi_i, & 0 \le t < T_1, \\ \psi_i + \left(\psi_f - \psi_i\right)\mathscr{B}_z(t, T_1, T_2), & T_1 \le t \le T_2, \\ \psi_f, & t > T_2, \end{cases} \tag{45}$$

where $\psi_i = 0$ rad, $\psi_f = 0.5$ rad, $T_1 = 0$ s, $T_2 = 5$ s, and $\mathscr{B}_z(t, T_1, T_2)$ is a Bézier interpolation polynomial given by

$$\mathscr{B}_z(t, T_1, T_2) = \frac{t - T_1}{T_2 - T_1}\left[r_1 - r_2\left(\frac{t - T_1}{T_2 - T_1}\right) + r_3\left(\frac{t - T_1}{T_2 - T_1}\right)^2 - \cdots + r_6\left(\frac{t - T_1}{T_2 - T_1}\right)^5\right], \tag{46}$$

with constants $r_1 = 252$, $r_2 = 1050$, $r_3 = 1800$, $r_4 = 1575$, $r_5 = 700$, and $r_6 = 126$.

Therefore, results show the proposed control approach simultaneously can properly reject disturbances and

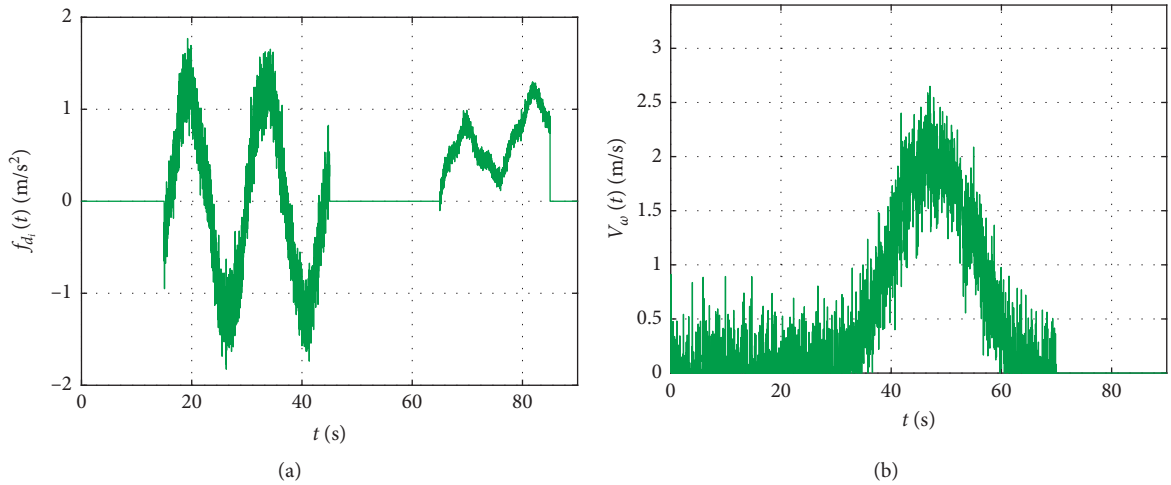

Figure 6: Wind disturbance representations. (a) Disturbance for $i = x; y; z$, case 1. (b) Wind speed model, case 2.

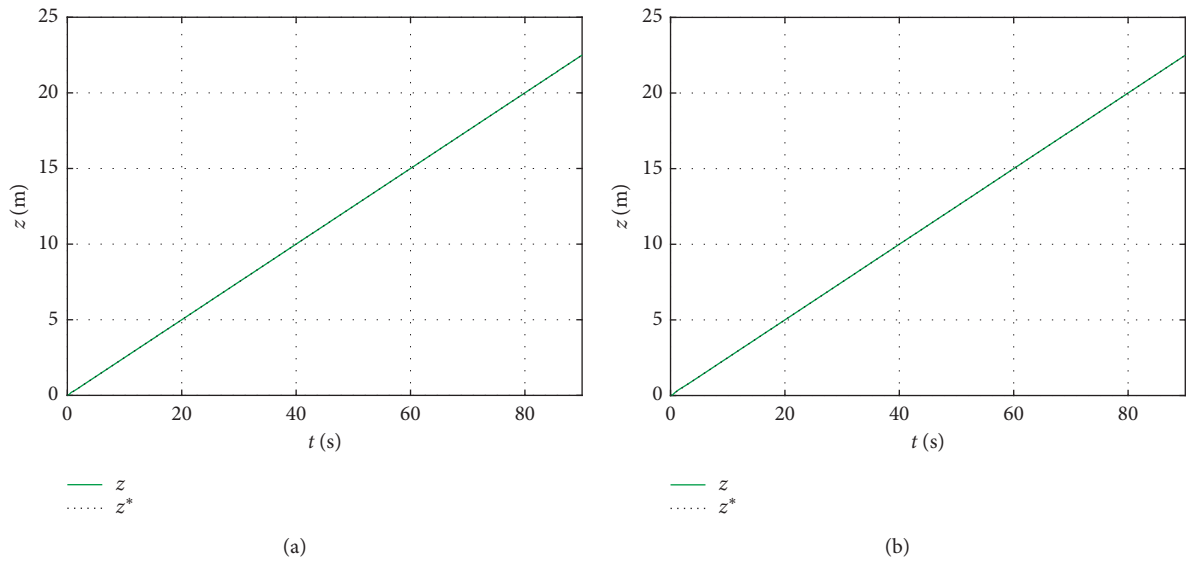

Figure 7: Tracking of planned reference trajectories for Z direction. (a) Trajectory tracking in (Z) case 1. (b) Trajectory tracking in (Z) case 2.

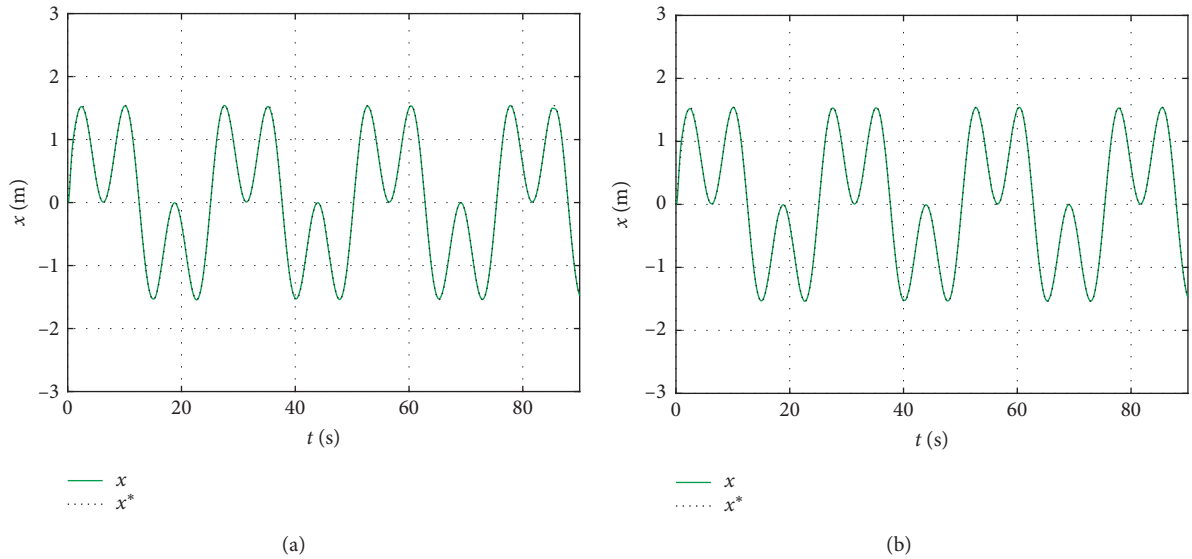

Figure 8: Continued.

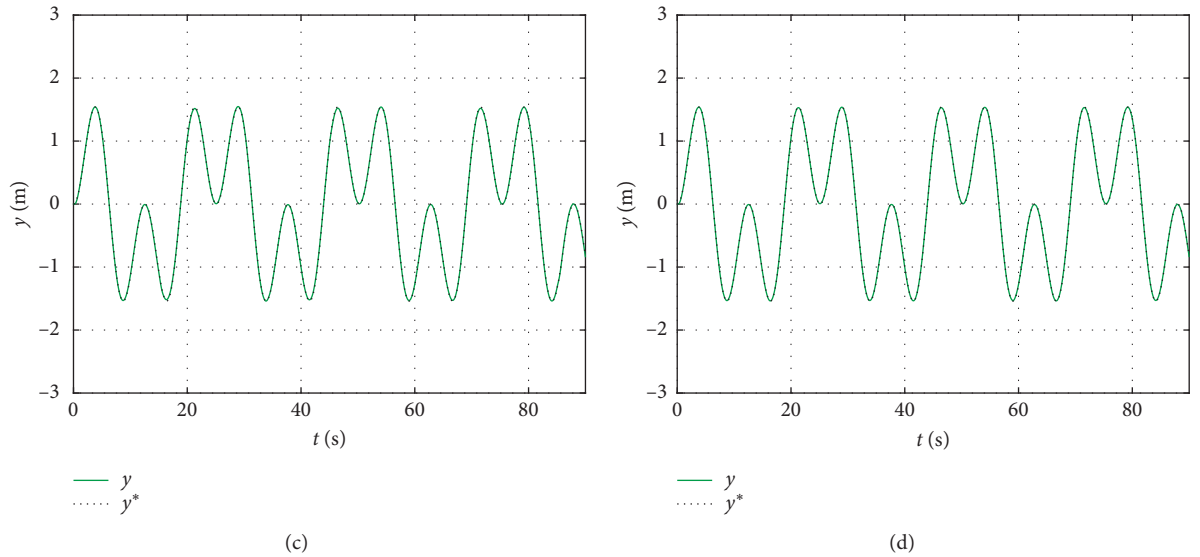

Figure 8: Tracking of planned reference trajectories for X and Y directions. (a) Trajectory tracking in X case 1. (b) Trajectory tracking in X case 2. (c) Trajectory tracking in Y, case 1. (d) Trajectory tracking in Y, case 2.

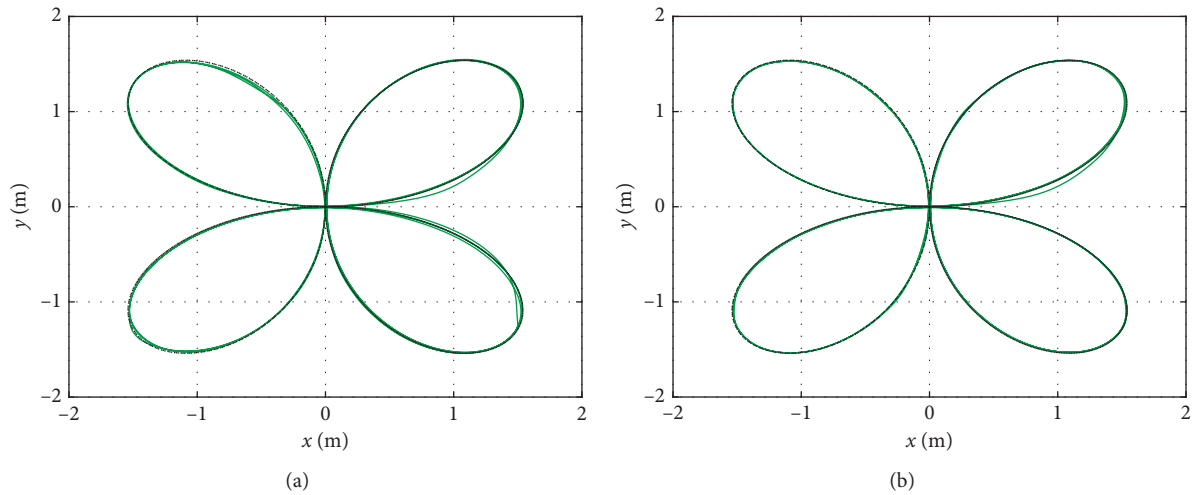

Figure 9: X-Y path followed by the quadrotor vehicle. (a) Path following case 1. (b) Path following case 2.

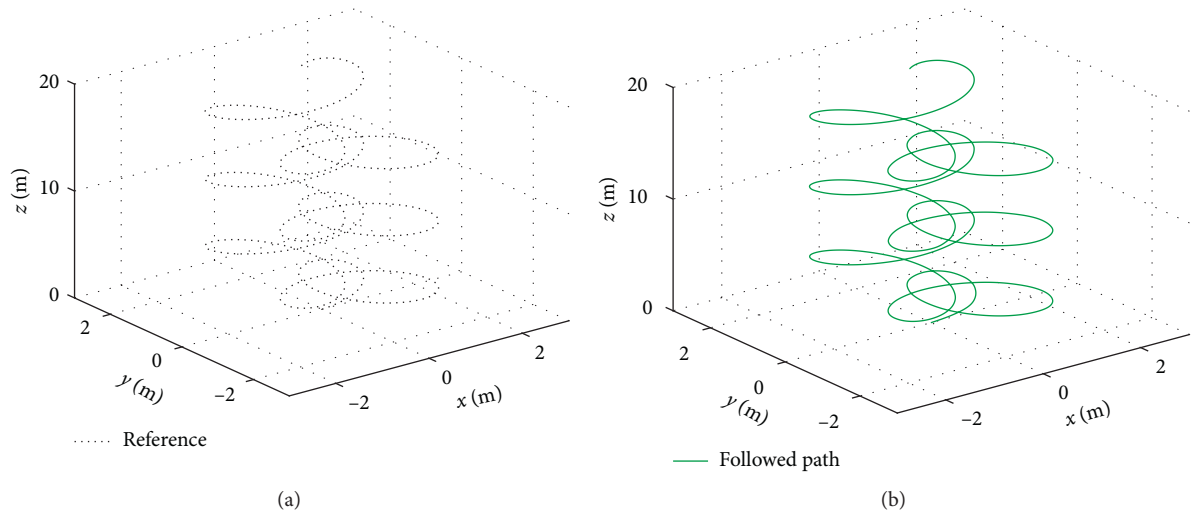

Figure 10: Following of the reference path specified for the controlled quadrotor motion, case 1.

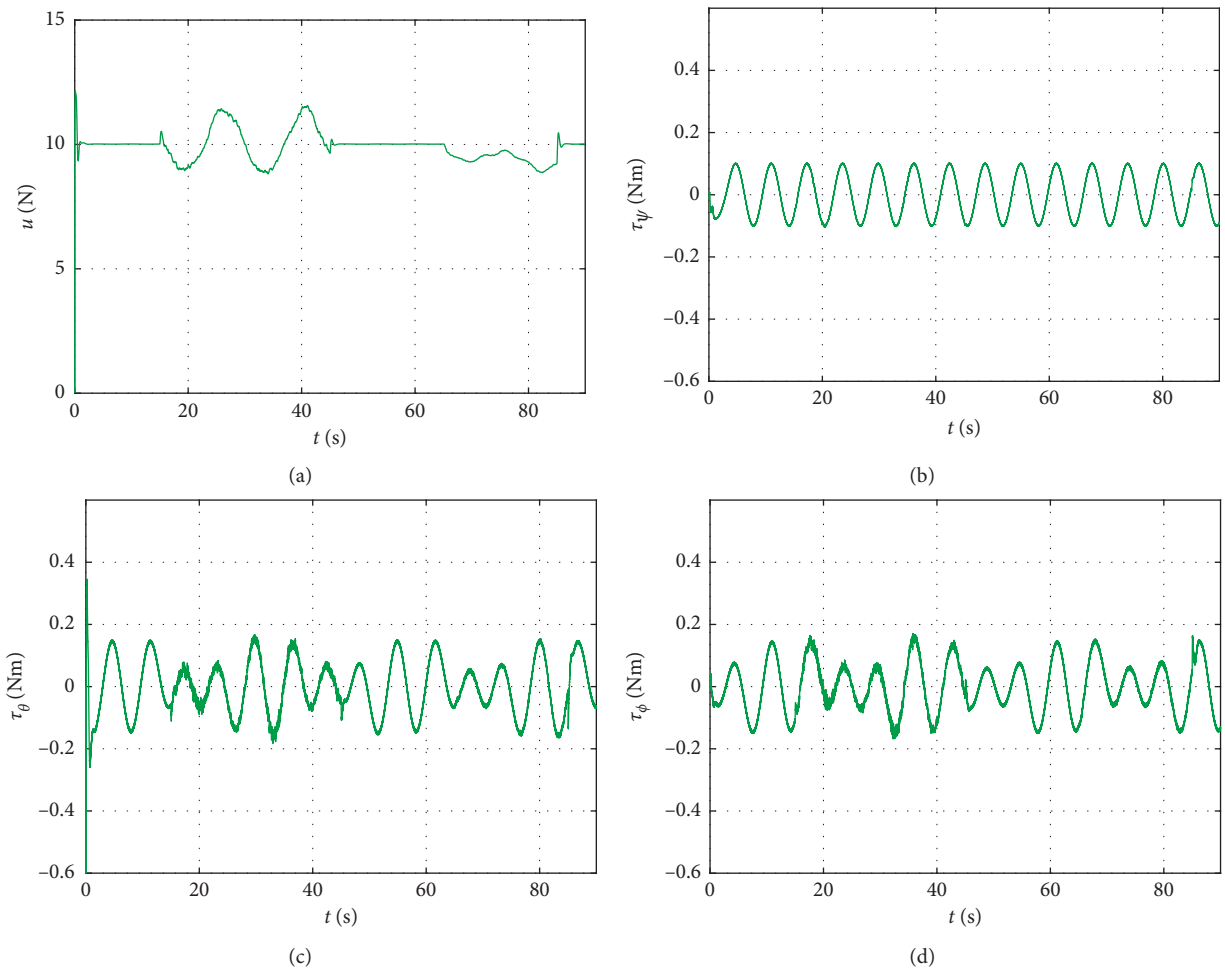

Figure 11: Computed robust control input signals for compensation of disturbances, case 1. (a) u. (b) τ_ψ. (c) τ_θ. (d) τ_φ.

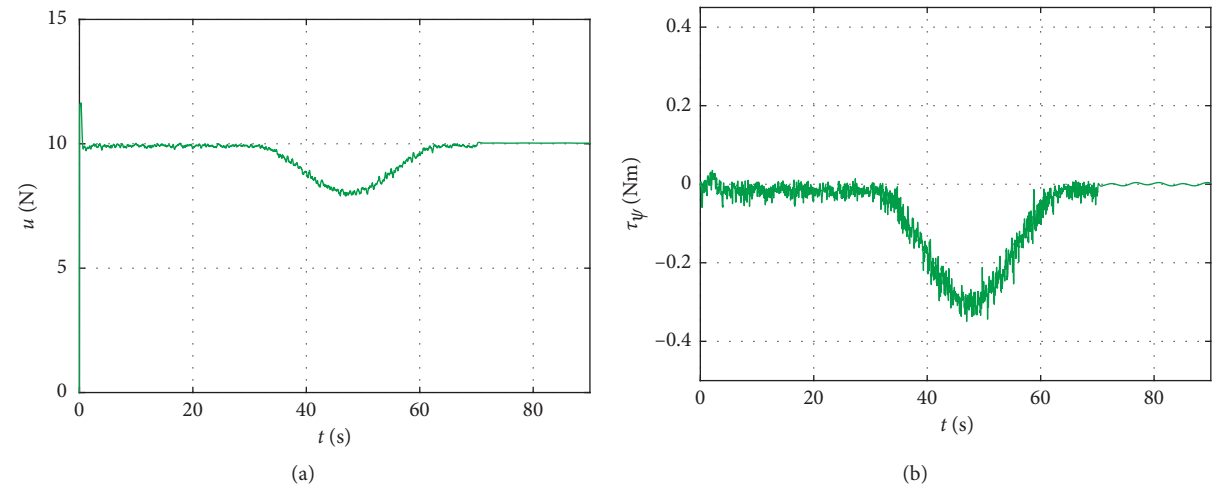

Figure 12: Continued.

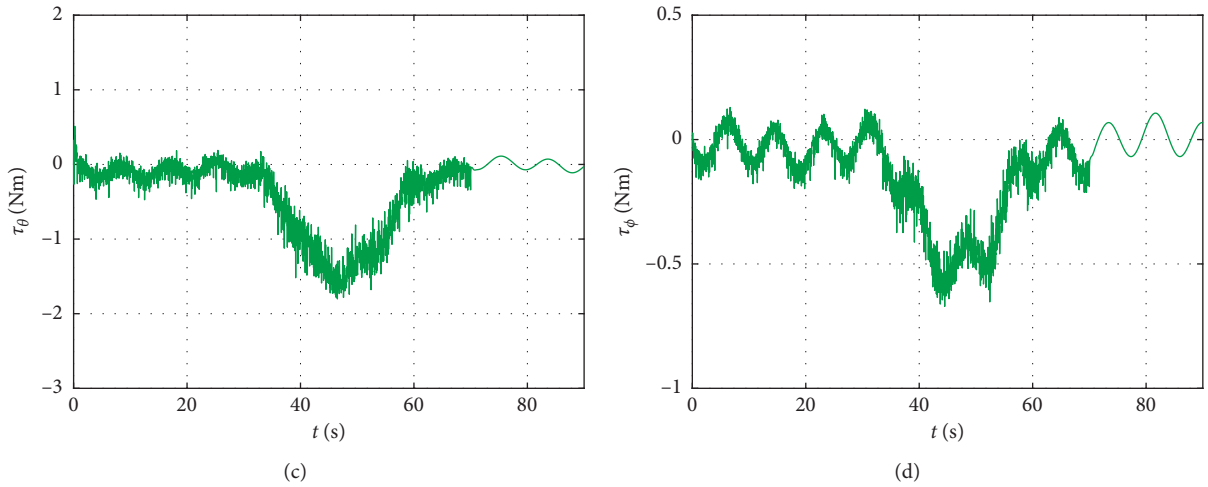

Figure 12: Computed robust control input signals for compensation of disturbances, case 2. (a) u. (b) τ_ψ. (c) τ_θ. (d) τ_φ.

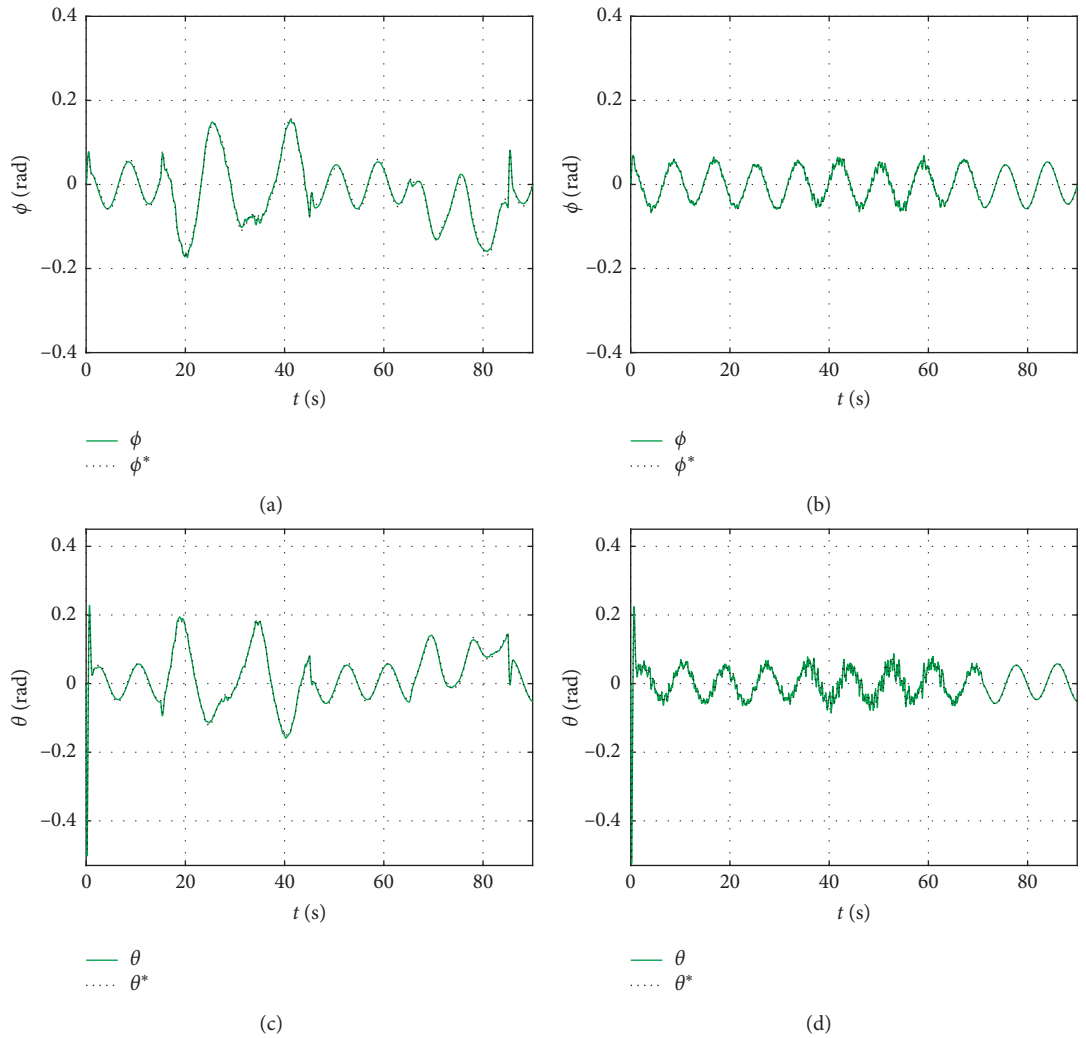

Figure 13: Continued.

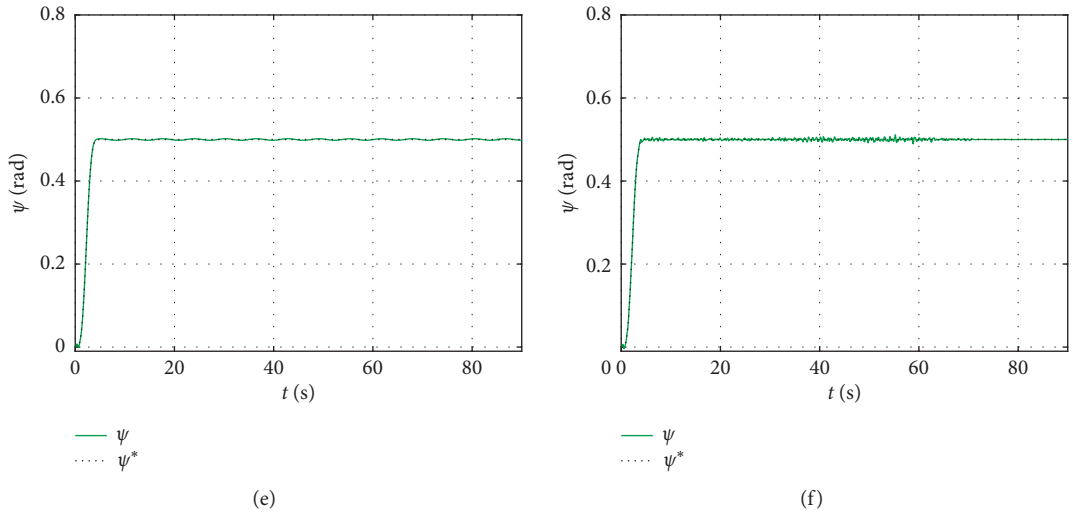

Figure 13: Tracking of planned reference trajectories for angular motion. (a) Trajectory tracking for φ, case 1. (b) Trajectory tracking for φ, case 2. (c) Trajectory tracking for θ, case 1. (d) Trajectory tracking for θ, case 2. (e) Trajectory tracking for ψ, case 1. (f) Trajectory tracking for ψ, case 2.

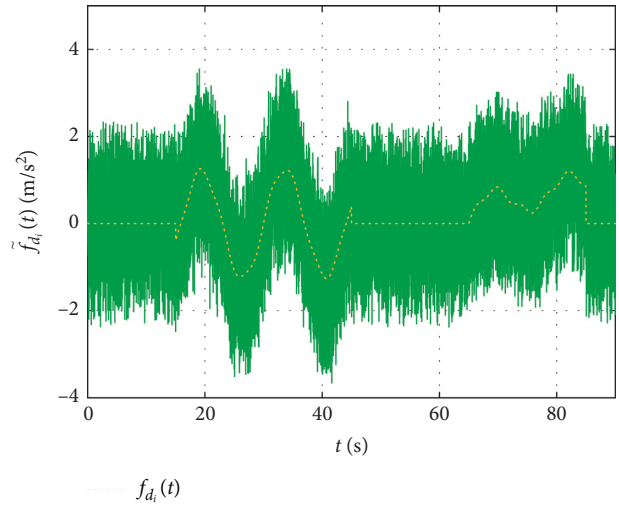

Figure 14: Acceleration disturbances induced by high-frequency motions.

perform an efficient tracking. Besides, notice from (33) that it is unnecessary to include the model information about the matrix Coriolis $\mathbf{C}(\dot{\eta}, \eta)$ as well as the angular nominal control trajectories $\ddot{\eta}^*$ in the controller design (36), which is desirable to keep the structure of the proposed controllers simple as possible.

Finally, a third case study is introduced to show the effectiveness and robustness of the proposed motion tracking control scheme against additional high-frequency time-varying disturbances depicted in Figure 14. Wide spectrum disturbances affecting the controlled aerial vehicle dynamics are described as

$$\xi_i = m\tilde{f}_{d_i}(t), \tag{47}$$

with

$$\tilde{f}_{d_i}(t) = f_{d_i}(t) + \mathcal{U}(0,1) + \mathcal{H}(n,t,\mathcal{A}). \tag{48}$$

Here, white noise generated by an uniform distribution $\mathcal{U}(0,1)$ in the interval $[0,1]$ was added. High-frequency harmonic components were also considered as

$$\mathcal{H}(n,t,\mathcal{A}) = \left[\mathcal{A}\sum_{j=1}^{n}\sin(100jt)\right] + \operatorname{sign}(\mathcal{N}(\mu,\sigma)) - 0.5, \tag{49}$$

with $\mathcal{A} = 0.5$ and $n = 3$. Furthermore, high-frequency unpredictable oscillations generated by a normal distribution $\mathcal{N}(\mu,\sigma)$, with mean value $\mu = 0$ and standard deviation $\sigma = 1$, were included.

Figure 15 portrays the robust control performance for following the 3D planned path. A satisfactory reference trajectory tracking can be observed in Figure 16, even though the quadrotor is subjected to high-frequency disturbance motions.

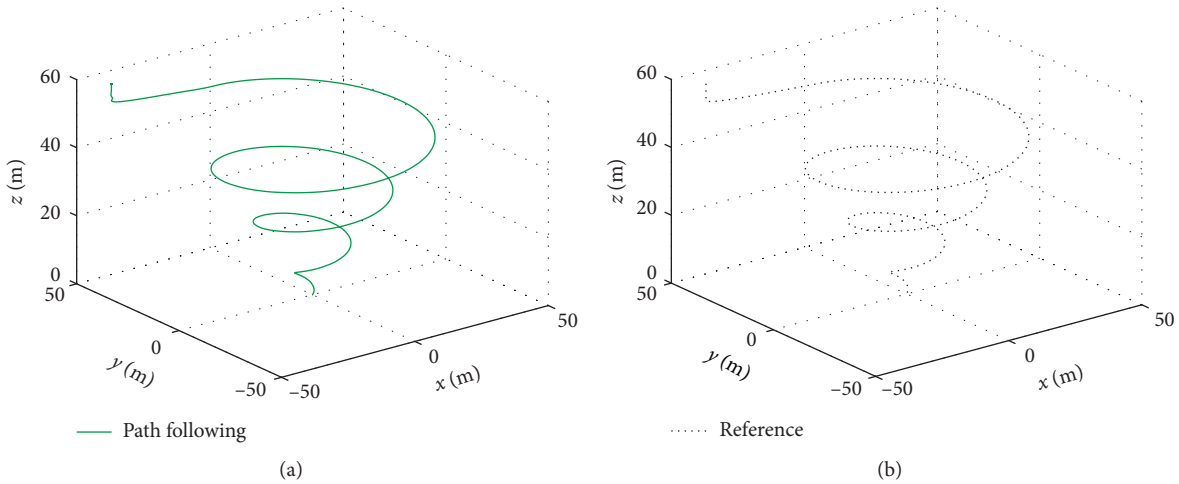

Figure 15: Satisfactory tracking of the reference path specified for the controlled quadrotor motion, case 3.

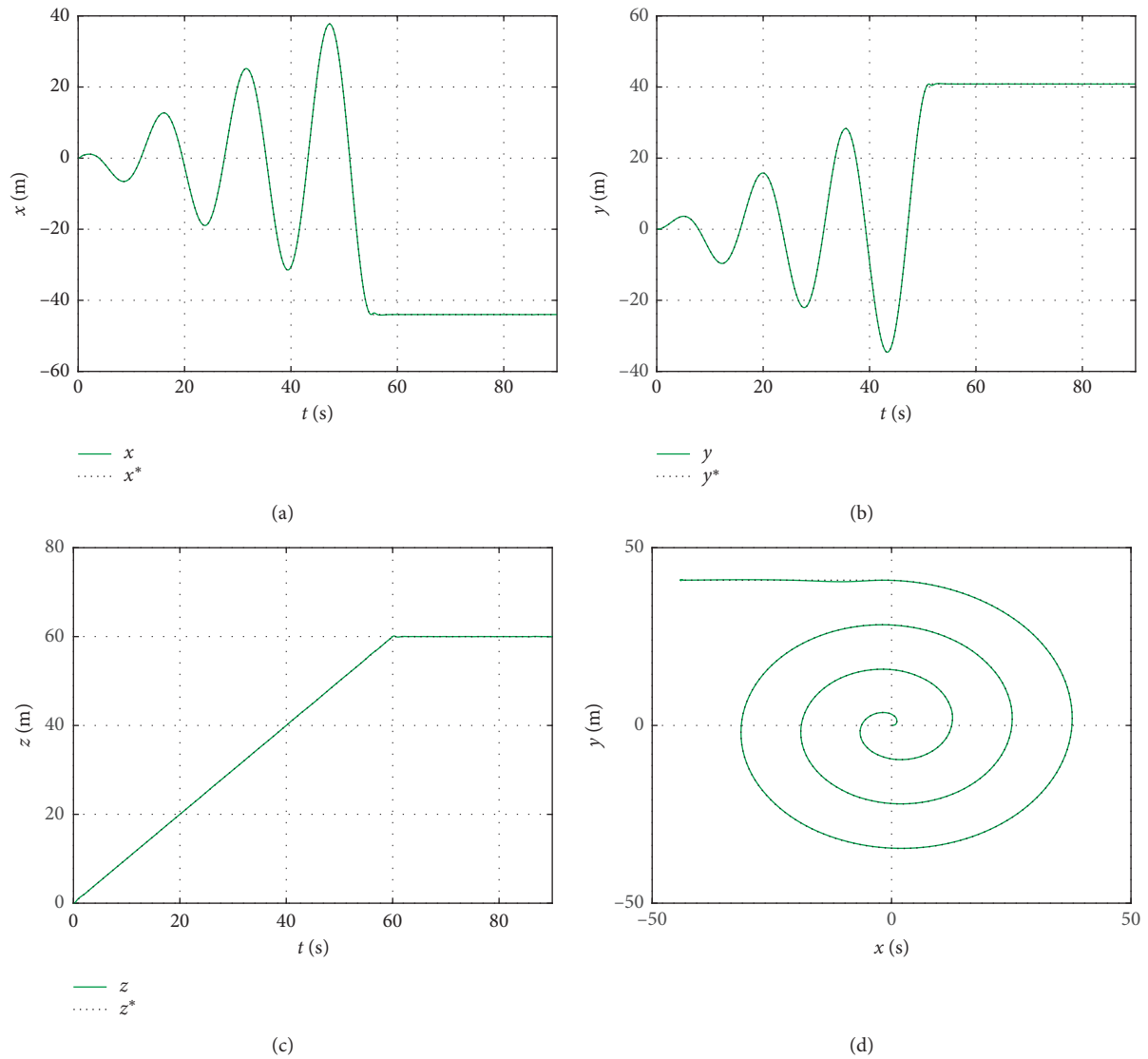

Figure 16: Tracking of the planned motion reference trajectories. (a) Trajectory tracking in X, case 3 (b) Trajectory tracking in Y, case 3 (c) Trajectory tracking in Z, case 3 (d) Path following, case 3.

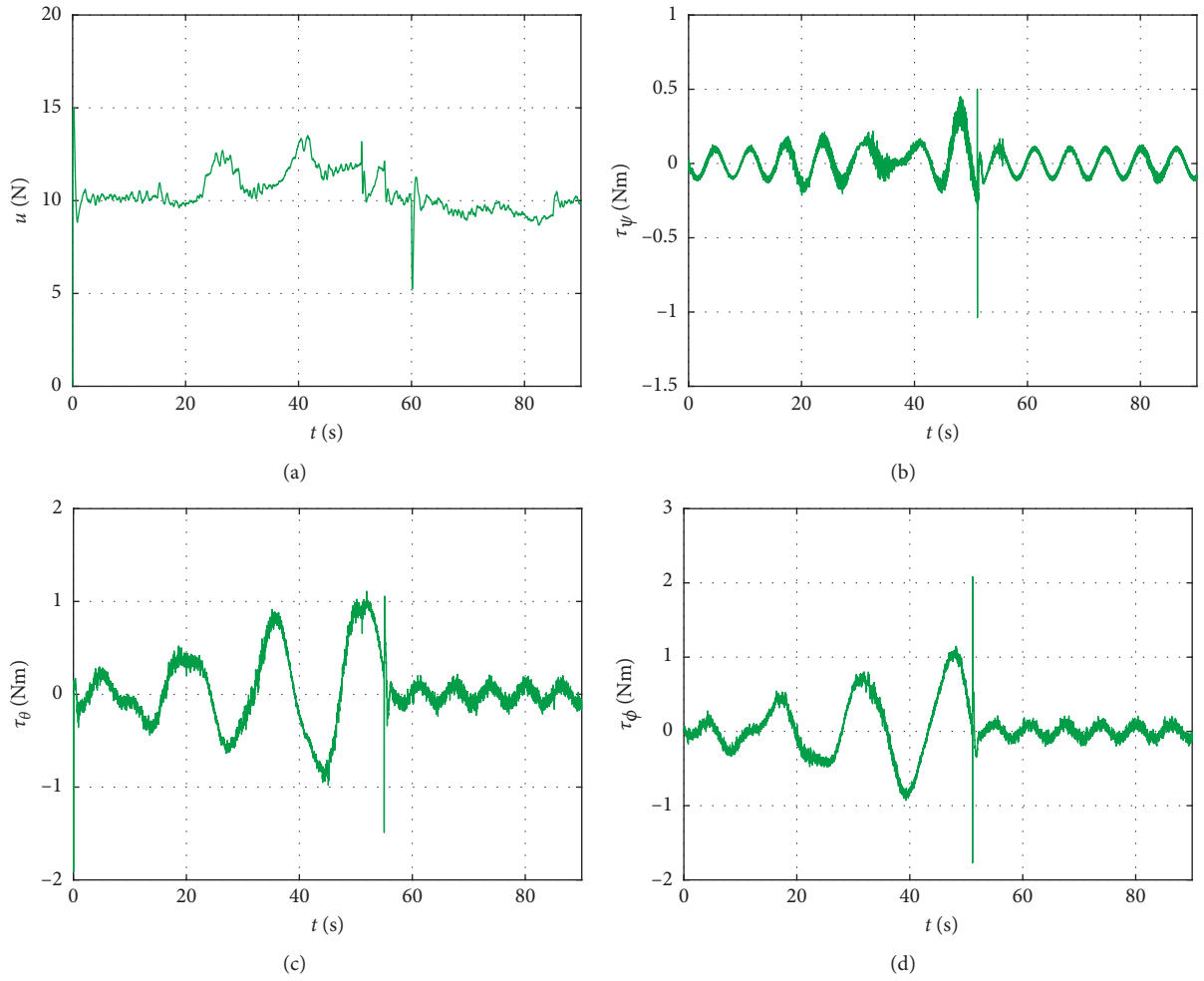

Figure 17: Robust control input signals computed in presence of high-frequency motion disturbances. (a) u. (b) τ_ψ. (c) τ_θ. (d) τ_φ.

Computed robust control inputs are shown in Figure 17. The high-frequency motion disturbance compensation is evident. Effectiveness and robustness of the dynamic controllers are hence confirmed. In this experiment, the reference for yaw motion was set as: $\psi^* = 0$ rad. From yielded results, it can be verified that the proposed dynamic motion tracking control is able to safely drive the quadrotor in the three-dimensional space in presence of undesirable high-frequency motions. It can be also corroborated that the quadrotor control achieves an acceptable trajectory tracking under reasonable time-varying operational uncertainties.

6. Conclusions

A novel and effective method based on active suppression of external and internal uncertainties for controlling the stable flight of a quadrotor helicopter in highly disturbed operating environments was introduced. A solution alternative for robust and efficient motion trajectory tracking tasks for an underactuated nonlinear aerial quadrotor vehicle under relevant uncertainties, from an active disturbance rejection perspective, has been proposed. Trajectory tracking is satisfactorily achieved by the controlled quadrotor. Main differences of the proposed desired motion tracking control approach with other important contributions have been highlighted. Robust asymptotic state observers for real-time estimation of disturbances and time derivatives are unnecessary. Dependence on detailed mathematical models of the complex nonlinear unmanned aerial system dynamics is considerably reduced. Two virtual controllers were designed to face the underactuated motion problem, and consequently, perform a suitable tracking of the planned references. Proposed dynamic compensators are able to actively reject disturbances in real time. Output signal measurements are only required for a proper tracking of the planned trajectories. Three strict case studies confirmed the robustness and efficiency of the proposed motion control scheme under hostile operating conditions. It was also proved that the presented active control approach can be directly extended for a class of vibrating mechanical systems. Therefore, analytical, experimental, and numerical results proved that the introduced motion trajectory tracking control method stands for a very good alternative to actively suppress disturbances. Future research works deal with the extension of the presented control design perspective to other nonlinear configurations of dynamically underactuated helicopters with multiple rotors operating

under uncertainty. In this context, effects of significant uncertainties and analysis of the transient behaviour of several controlled multirotor aerial vehicles will be considered in future works as well.

Data Availability

The data used to support the findings of the study are available from the corresponding author upon request.

Conflicts of Interest

The authors declare that they have no conflicts of interest.

References

[1] B. Siciliano and O. Khatib, *Springer Handbook of Robotics*, Springer International Publishing, Berlin, Germany, 2nd edition, 2016.

[2] X. Shao, N. Liu, Z. Wang, W. Zhang, and W. Yang, "Neuroadaptive integral robust control of visual quadrotor for tracking a moving object," *Mechanical Systems and Signal Processing*, vol. 136, Article ID 106513, 2020.

[3] P. Castillo, R. Lozano, and A. Dzul, *Modelling and Control of Mini-Flying Machines*, Springer Publishing Company, Inc., New York, NY, USA, 1st edition, 2010.

[4] P. Corke, *Robotics, Vision and Control: Fundamental Algorithms in MATLAB*, Springer Publishing Company, New York, NY, USA, 2nd edition, 2017.

[5] S. Bouabdallah, A. Noth, and R. Siegwart, "PID vs LQ control techniques applied to an indoor micro quadrotor," in *Proceedings of the 2004 IEEE/RSJ International Conference on Intelligent Robots and Systems (IROS)*, vol. 3, pp. 2451–2456, Sendai, Japan, October 2004.

[6] G. Hoffmann, H. Huang, S. Waslander, and C. Tomlin, "Quadrotor helicopter flight dynamics and control: theory and experiment," in *Proceedings of the AIAA Guidance, Navigation and Control Conference and Exhibit, American Institute of Aeronautics and Astronautics*, pp. 1670–1689, Hilton Head, SC, USA, August 2007.

[7] A. A. Mian and W. Daobo, "Modeling and backstepping-based nonlinear control strategy for a 6 DOF quadrotor helicopter," *Chinese Journal of Aeronautics*, vol. 21, no. 1, pp. 261–268, 2008.

[8] A. Modirrousta and M. Khodabandeh, "A novel nonlinear hybrid controller design for an uncertain quadrotor with disturbances," *Aerospace Science and Technology*, vol. 45, pp. 294–308, 2015.

[9] A. Noormohammadi-Asl, O. Esrafilian, M. Ahangar Arzati, and H. D. Taghirad, "System identification and $H\infty$-based control of quadrotor attitude," *Mechanical Systems and Signal Processing*, vol. 135, Article ID 106358, 2020.

[10] Z. Cai, J. Lou, J. Zhao, K. Wu, N. Liu, and Y. X. Wang, "Quadrotor trajectory tracking and obstacle avoidance by chaotic grey wolf optimization-based active disturbance rejection control," *Mechanical Systems and Signal Processing*, vol. 128, pp. 636–654, 2019.

[11] J. Han, "From PID to active disturbance rejection control," *IEEE Transactions on Industrial Electronics*, vol. 56, no. 3, pp. 900–906, 2009.

[12] Z. Gao, "Active disturbance rejection control: a paradigm shift in feedback control system design," in *Proceedings of the 2006 American Control Conference*, pp. 2399–2405, Minneapolis, MN, USA, June 2006.

[13] J. Li, R. Li, and H. Zheng, "Quadrotor modeling and control based on linear active disturbance rejection control," in *Proceedings of the 2016 35th Chinese Control Conference (CCC)*, pp. 10651–10656, Chengdu, China, July 2016.

[14] H. Lu, X. Zhu, C. Ren, S. Ma, and W. Wang, "Active disturbance rejection sliding mode altitude and attitude control of a quadrotor with uncertainties," in *Proceedings of the 2016 12th World Congress on Intelligent Control and Automation (WCICA)*, pp. 1366–1371, Guilin, China, June 2016.

[15] R. Sanz, P. Garcia, and P. Albertos, "Active disturbance rejection by state feedback: experimental validation in a 3-DOF quadrotor platform," in *Proceedings of the 2015 54th Annual Conference of the Society of Instrument and Control Engineers of Japan (SICE)*, pp. 794–799, Hangzhou, China, July 2015.

[16] W. Dong, G.-Y. Gu, X. Zhu, and H. Ding, "A high-performance flight control approach for quadrotors using a modified active disturbance rejection technique," *Robotics and Autonomous Systems*, vol. 83, pp. 177–187, 2016.

[17] M. Fliess, R. Marquez, E. Delaleau, and H. Sira–Ramírez, "Correcteurs proportionnels-intégraux généralisés," *ESAIM: Control, Optimisation and Calculus of Variations*, vol. 7, pp. 23–41, 2002.

[18] F. Beltran-Carbajal and G. Silva-Navarro, "Generalized nonlinear stiffness identification on controlled mechanical vibrating systems," *Asian Journal of Control*, vol. 21, no. 3, pp. 1281–1292, 2019.

[19] F. Beltran-Carbajal, G. Silva-Navarro, and L. G. Trujillo-Franco, "A sequential algebraic parametric identification approach for nonlinear vibrating mechanical systems," *Asian Journal of Control*, vol. 19, no. 4, pp. 1564–1574, 2017.

[20] F. Beltran-Carbajal, R. Tapia-Olvera, I. Lopez-Garcia, A. Valderrabano-Gonzalez, J. C. Rosas-Caro, and J. L. Hernandez-Avila, "Extended PI feedback tracking control for synchronous motors," *International Journal of Control, Automation and Systems*, vol. 17, no. 6, pp. 1346–1358, 2019.

[21] F. Beltran-Carbajal, A. Favela-Contreras, J. L. Hernandez-Avila, O. Olvera-Tapia, D. Sotelo, and C. Sotelo, "Dynamic output feedback control for desired motion tracking on synchronous motors," *International Transactions on Electrical Energy Systems*, vol. 30, no. 3, Article ID e12260, 2020.

[22] S. Elias, R. Rupakhety, and S. Olafsson, "Analysis of a benchmark building installed with tuned mass dampers under wind and earthquake loads," *Shock and Vibration*, vol. 2019, Article ID 7091819, 13 pages, 2019.

[23] B. G. Korenev and L. M. Reznikov, *Dynamic Vibration Absorbers: Theory and Technical Applications*, John Wiley & Sons, England, UK, 1993.

[24] A. Yanik, "Absolute instantaneous optimal control performance index for active vibration control of structures under seismic excitation," *Shock and Vibration*, vol. 2019, Article ID 4207427, 13 pages, 2019.

[25] P. Castillo, P. García, R. Lozano, and P. Albertos, "Modelado y estabilización de un helicóptero con cuatro rotores," *Revista Iberoamericana De Automática e Informática Industrial RIAI*, vol. 4, no. 1, pp. 41–57, 2007.

[26] P. Castillo, L. E. Muñoz, and O. Santos, "Robust control algorithm for a rotorcraft disturbed by crosswind," *IEEE Transactions on Aerospace and Electronic Systems*, vol. 50, no. 1, pp. 756–763, 2014.